Journal of Materials Science: Materials in Electronics (2019) 30:16789–16797
https://doi.org/10.1007/s10854-019-01337-6

Synthesis and characterization of aminolevulinic acid with gold and iron nanoparticles by photoreduction method for non-communicable diseases diagnosis and therapy

Karina de Oliveira Gonçalves[1,2] · Flávia Rodrigues de Oliveira Silva[3] · Daniel Perez Vieira[2] · Lilia Coronato Courrol[1]

Received: 17 October 2018 / Accepted: 15 April 2019 / Published online: 22 April 2019

Abstract
Non-communicable diseases (NCDs) are a group of chronic diseases resulted by genetic, epigenetic and environmental factors and life style. The main types of NCDs are cardiovascular diseases and cancers. Some of therapeutic treatments for NCDs induce severe cytotoxicity to normal cells. New treatments as photodynamic and sonodynamic therapies have been proposed trying to improve the cure rate and reduce the side-effects. In these treatments certain drugs as porphyrins precursors associated to metal nanoparticles (MNPs) have become of extreme interest since have high targeting ability and potentiality to destroy tumor tissues. MNPs can induce cell death through various processes, including reactive oxygen species (ROS) generation and DNA damage, among others. In this work, we describe synthesis of MNPs by photoreduction with aminolevulinic acid (ALA), a protoporphyrin IX precursor. To obtain ALA:MNPs (M = Au or/and Fe), ALA, polyethylene glycol, and Tetrachloroauric acid and/or iron powder water solutions were irradiated by Xenon lamp. The UV–vis spectra, transmission electron microscopy and zeta potential were measured to characterize nanoparticles. The proposed mechanism of nanoparticle formation was described from a physicochemical perspective. The THP-1 macrophages cytotoxicity was determined, and photodynamic therapy (PDT) with high power LED at 590 nm for 2 min were performed. The results have suggested that the gold/iron nanoparticles interfere in the selectivity of iron transport across the mitochondrial inner membrane and enhance the effectiveness of the PDT acting as important agent for NCDs control.

1 Introduction

Non-communicable diseases (NCDs), mainly cardiovascular diseases (CDVs) and cancer, are quickly becoming the world's greatest health issue [1]. Shared features of atherosclerosis, the main cause of CDVs, and cancer, as oxidative stress, inflammation, proliferation and angiogenesis, justify similar approaches to diagnosis and therapy [2].

In this context, new treatments as photodynamic therapy (PDT) have been proposed trying to improve the cure rate and reduce the side-effects of tumor-like diseases [3–5]. In PDT, three components are necessary to promote tumor destruction: a photosensitizer, light, and oxygen. After excitation of sensitizer by photons, a sequence of internal conversion, intersystem crossing and electron or energy transfer to oxygen molecules present in the medium, culminates with the production of reactive oxygen species, which damage membranes and organelles, causing cell death [6]. One of the most commonly used photosensitizer is 5-aminolevulinic acid (ALA), the biological precursor of protoporphyrin IX (PpIX) [7]. ALA administration upregulates heme synthesis leading to the induction of hemoprotein synthesis. Previous studies have demonstrated that ALA selectively accumulates in macrophages and foam cells in atherosclerotic plaques [8–10]. Extensive studies have been indicated that tumors and other proliferating cells tend to exhibit a higher level of PpIX than normal cells after ALA incubation [11–13]. PpIX was found accumulated in the cytoplasm of THP-1 macrophages [14].

The gold nanoparticles can act as carriers of ALA improving PDT efficiency [15, 16]. Gold nanoparticles (AuNPs) are easy to synthesize, possess unique, tunable

✉ Lilia Coronato Courrol
lccourrol@gmail.com

[1] Departamento de Física, Universidade Federal de São Paulo, Diadema, SP, Brazil

[2] Centro de Biotecnologia, Instituto de Pesquisas Energéticas e Nucleares, São Paulo, SP, Brazil

[3] Centro de Ciência e Tecnologia de Materiais, Instituto de Pesquisas Energéticas e Nucleares, São Paulo, SP, Brazil

optical properties, due to the localized surface plasmon resonance (SPR) [17, 18], and excellent biocompatibility. Can be used also in photothermal ablation and drug delivery [17, 19, 20].

The Nanohybrids (NH) are materials that contain multicomponent or hierarchical structures where two or more elements are conjugated [21]. The NH synthesis and use present challenges and results in physical and chemical modification of nanomaterials.

Size, structure, shape and functionalization of NH generate novel advantages. For example, nanoscale iron oxide possesses paramagnetic characteristics and gold nanoparticles have plasmon resonance properties [22, 23]. The incorporation of gold and iron into a nanoparticle structure can potentially enhance the optical/plasmonic and magnetic properties of the material [24]. The multifunctional NH can be used as magnetic resonance imaging (MRI) agents with added nanoheating properties, useful for laser irradiated drug delivery systems [24]. When exposed to an external magnetic field, NH can be transferred purposely to a position and may thus act as an effective drug [22, 25].

Typical synthesis of nanohybrids are based on the co-precipitation of metal salts or reverse micelle methods [23, 26]. Studies have reported on the utilization of physical methods for nanohybrids synthesis for example using pulsed laser ablation in liquids [26]. Recently green approach using photoreduction has been described in many synthesis procedures of nanoparticles [27–29].

In this study, the selected method to synthetize nanohybrids was the photoreduction using ALA, polyethylene glycol (PEG) and ligth. The synthesized nanohybrids were characterized and toxicity was evaluated in macrophage-differentiated THP-1 cells. PDT were performed. The obtained results can evaluate the applicability of nanohybrids in NCDs diagnosis and therapy.

2 Materials and methods

2.1 Materials

$HAuCl_4$, polyethylene glycol (PEG) and aminolevulinic acid (ALA), were purchased from Sigma Aldrich and iron powder, from Cidepe, Centro Industrial de Ensino e Pesquisa Ltda, Brazil. All chemicals were of analytical grade and used as received. The water used in the experiments was deionized.

2.2 Synthesis of ALA:Au

First, $HAuCl_4$, ALA and PEG were mixed in deionized water. The concentrations of the reagents used are described in the Table 1. Then, the solution was exposed to a 300 W Cermax Xenon Lamp by 2 min. The lamp was positioned 10 cm away from the recipient containing the solution, and the illuminated region covered exactly the recipient diameter, with a 3.6 W/cm^2 estimated intensity. The solution color gradually changed from light yellow to purple and finally to red.

Table 1 Concentration of reagents and time of exposure to light

Solution	Reagents	Irradiation time (min)
ALA + PEG	13.5 mg of ALA 20 mg of Polyethylene glycol (PEG) 30 mL	–
ALA + PEG + $HAuCl_4$	13.5 mg of ALA 45 mg of $HAuCl_4$ 20 mg of Polyethylene glycol (PEG) 30 mL	
ALA:Au	13.5 mg of ALA 45 mg of $HAuCl_4$ 20 mg of Polyethylene glycol (PEG) 30 mL	2 pH ~ 7.2
ALA:AuFe	45 mg of $HAuCl_4$ 13.5 mg of iron powder 13.5 mg of ALA 20 mg of PEG 30 mL pH before illumination ~ 12	2–5 pH ~ 7.4

2.3 Synthesis of nanohybrids ALA:AuFe

$HAuCl_4$, ALA, PEG and iron powder were mixed in deionized water with the concentrations described in the Table 1. The pH of solution was adjusted to 12. Following, the solution was exposed to Xe lamp. The solution color gradually changed from light yellow to dark purple. The pH was adjusted to ~ 7.0 after illumination.

2.4 Characterization

A 2600 Shimatzu Japan (UV–Vis) spectrophotometer was employed for acquisition of the solution's optical absorption spectra before and after illumination.

JEM 2100 (Jeol) transmission electron microscope (TEM), was employed to examine the nanoparticles morphologies. The images were captured by Gatan camera and processed by the software Digital Micrograph.

The hydrodynamic size and zeta potential distribution of the synthesized nanoparticles were determined using Nano-ZS90 (Malvern).

Fourier-transform infrared (FT-IR) spectra were recorded in the wavenumber range from 400 to 4000 cm^{-1} using a

Shimatzu IR Prestige-21. In this case, 300 µL of solutions were deposited on microscope slides and left in the desiccator by 24 h. The dried material was used for the preparation of a KBr pellet for analysis.

2.5 Cell culture

THP-1 cells have become one of most widely used cell lines to investigate the function and regulation of monocytes and macrophages in the cardiovascular system [30]. In our case THP-1 cells were used to model atherosclerosis in vitro. Human monocytic leukemia THP-1 cells (Sigma Aldrich) were cultured in RPMI-1640 medium. Cells were seeded at 5000 cells per well in 96-well plates and incubated at 37 °C in a humidified atmosphere of 5% CO_2 in 95% air. THP-1 cells were treated with 75 ng/mL of phorbol myristate acetate (PMA, Sigma-Aldrich Co., St, Louis, MO, USA) for 48 h to induce differentiation of the cells into macrophages. After differentiation, non-attached cells were removed by aspiration and the adherent macrophages were washed with RPMI-1640 medium three times and then incubated in cell culture medium at 37 °C.

2.6 Cell viability assay

Cytotoxicity evaluation of nanoparticles was performed using MTS assay. The THP-1 cells were incubated with ALA (10 µL), ALA:AuNPs (10, 20, 30 and 40 µL) and ALA:AuFeNPs (10, 20, 30 and 40 µL) by 24 h in dark. The volume in each well in 96-well plate was kept constant by addition of RPMI-1640 medium. After 24 h the cells were washed several times with phosphate buffered saline (PBS) (pH = 7.2–7.6). The ALA-free cells were suspended in 100 µL media and assayed for viability using the colorimetric MTS assay kit based on the CellTiter 96 Aqueous One Solution (Promega, Madison, WI, USA). In this procedure, the cells were incubated with fresh medium containing MTS reagent for 2 h before measurements at an absorbance of 490 nm. The effect of particles on cell viability was expressed as percentage of inhibition of cell growth relative to the control. Results were statistically compared (ANOVA and Bonferroni post-test) to negative (control cells, NaCl 0.9%) or positive (latex extract, 0.5 g/L in culture media, 24 h) controls. In this experiment n = 4 for Latex, NaCl and control groups and n = 9 for ALA groups.

2.7 PDT procedures

The cells followed the protocol described above, and after differentiation, macrophages were incubated with culture medium ALA:AuNPs (10 µL) and ALA:AuFeNPs (10 µL) for 24 h.

The LED, 590 nm, high intensity (MM Optics Brazil) was placed below the plate containing cells. The cells groups were irradiated separately during 2 min.

After PDT treatment, the cells were washed with PBS and were incubated with fresh medium containing MTS reagent for 4 h before measurements at 490 nm. In this experiment n = 4 for Latex, n = 3 for NaCl, n = 6 for control group and n = 12 for ALAAuNPs + PDT and ALA:AuFeNPs + PDT groups.

3 Results

Color of gold colloid is attributed to surface plasmon resonance (SPR) arising due to the collective oscillation of free conduction electrons induced by an interacting electromagnetic field. The color change from pale yellow to purple pink color and finally red was observed during the illumination by Xenon lamp for 2 min of water solutions containing, ALA, HAuCl4, PEG (Fig. 1a). PEG

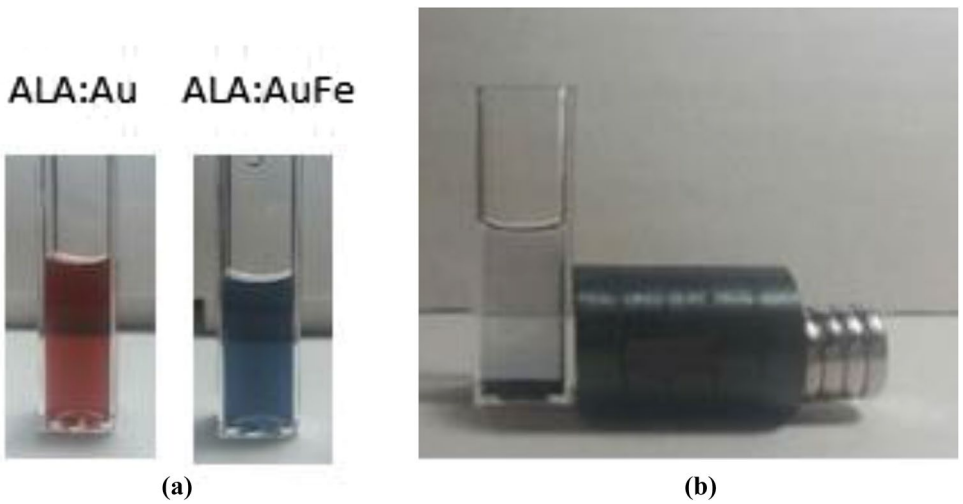

Fig. 1 **a** Aspect of ALA:Au and ALA:AuFeNPs solutions. **b** A magnet was placed next to the cuvette containing ALA:AuFeNPs solution for 10 min, evidencing the magnetization of nanoparticles

is commonly used to functionalize the surface of gold nanoparticles (AuNPs) in order to improve their in vivo stability. Addition of iron powder in the solution containing $HAuCl_4$ (pH = 12) promoted changes in the solutions colors to blue/dark purple as showed in the Fig. 1a. In the Fig. 1b, gold/iron irradiated solution attracted by a magnet indicating magnetization.

The Fig. 2 shows the results of the UV–Vis spectra measurements obtained for ALA + PEG, ALA + PEG + $HAuCl_4$, ALA:AuNPs and ALA:AuFeNPs described in the Table 1. In this figure it is possible to observe the presence of a peak around 300 nm due to the presence of auric complexes. The peak around 536 nm for ALA:AuNPs illuminated by 2 min is due to the surface plasmon resonance, characteristic of gold nanoparticles. The presence of iron in plasmon coupling of gold results in suppression of band around 300 nm and a shift of the extinction peak to higher wavelengths (548 nm) as the interparticle spacing is reduced. Higher the illumination time, smaller is the SPR intensity indicating decrease of concentration of gold nanoparticles in nanohybrids structure. Apart from the red shift of SPR band, Fig. 2 shows a new broad absorption band at around 750 nm in ALA:AuFeNPs.

Xenon lamp radiates over a wide spectral range, from the ultraviolet to the infrared and solution temperature increases with illumination. The photoreduction process promotes the reduction of gold ions (Au^{3+}) into metallic gold (Au^0):

$$Au^{3+} + 3e^- \rightarrow Au^0, E^{\circ}_{red} = 1.40\ V.$$

With the reduction to Au^0, there is the formation of gold clusters. The presence of ALA and PEG suppresses the agglomeration of gold particles stabilizing the colloidal suspension and cover the nanoparticles.

The photoreduction process in the solution containing $HAuCl_4$, PEG and iron powder promoted an irreversible inter-particle coupling accompanied by a red-shift in the spectrum of AuNPs, as well as broadening and decrease in the intensity of SPR band.

Iron occurs in the divalent or ferrous form and the trivalent or ferric form. Iron in aqueous solution is subject to hydrolysis producing the iron hydroxides, especially the ferric form that have very low solubility. Under oxidizing conditions (ph ~ 12), practically all the iron is precipitated as ferric hydroxide.

$$3Fe(OH)_2 \rightarrow Fe_3O_4 + H_2 + 2H_2O$$

Iron nanoparticles (Fe_3O_4) are stabilized by ALA and PEG.

Figure 3 shows the FTIR spectra in the region of 4000 to 400 cm^{-1} obtained from dried films of PEGylated ALA:AuNPs and ALA:AuFeNPs. The PEG spectrum shows characteristic bands of specific functional groups, such as the bands appearing at 2881 cm^{-1} assigned to the –CH group and the band at 1103 cm^{-1} assigned to the –C–O–C group [31]. A characteristic peak at about 3428 cm^{-1} representing vibration N–H of PEG was evident in the spectra of ALA:AuNPs and ALA:AuFeNPs. For ALA, 1716 cm^{-1} band can be associated to C=O group. A very small band was observed around 592 cm^{-1} and can be assigned to the Fe–O stretching vibration for the iron nanoparticles.

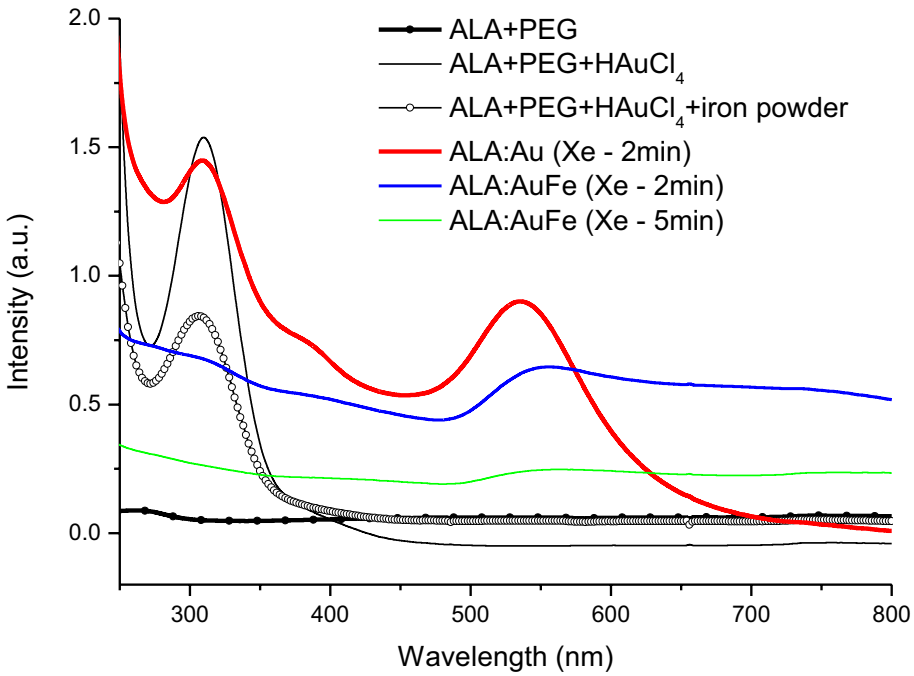

Fig. 2 Uv–Vis spectra of prepared solutions: ALA + PEG, ALA + PEG + $HAuCl_4$ and ALA + PEG + $HAuCl_4$ + iron powder without illumination; ALA + PEG + $HAuCl_4$ (ALA:Au) and ALA + PEG + $HAuCl_4$ + iron powder (ALA:AuFe) irradiated by 2 min and ALA + PEG + $HAuCl_4$ + iron powder (ALA:AuFe) irradiated by 5 min

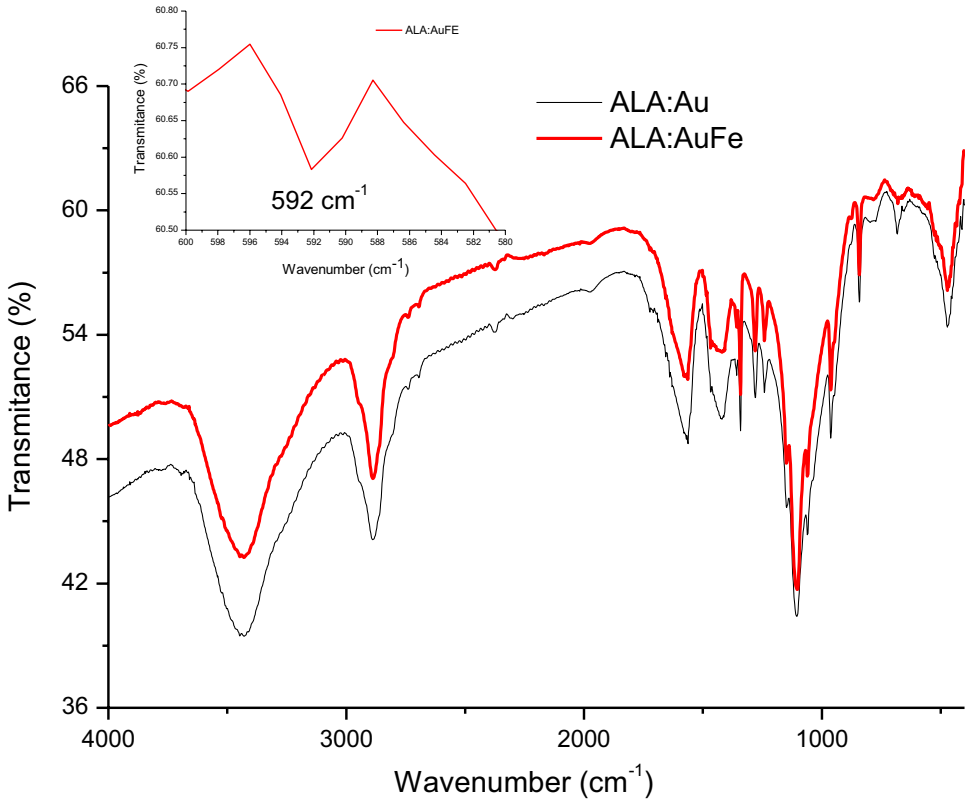

Fig. 3 FTIR spectra of PEGylated ALA:AuNPs and ALA:AuFeNPs solutions

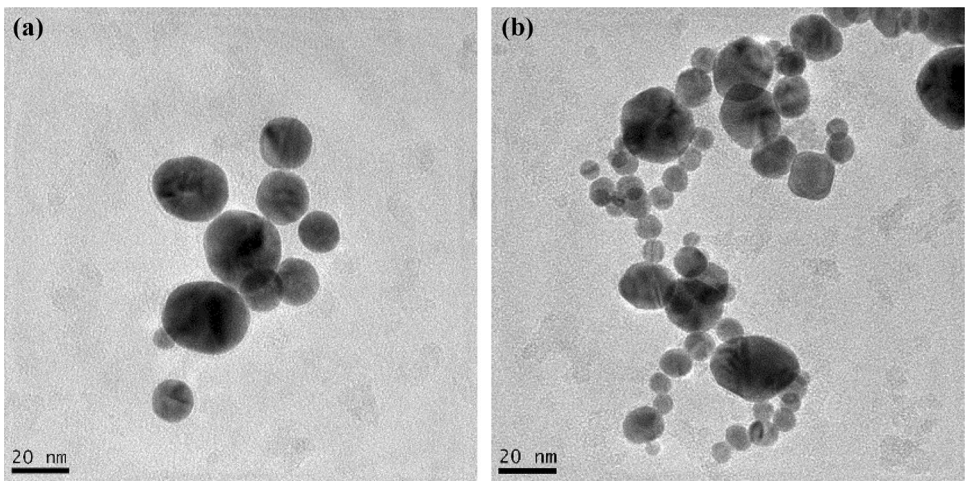

Fig. 4 Transmission electron microscopy of solutions: **a** ALA:AuNps (2 min Xe) and **b** ALA:AuFeNPs (2 min Xe)

Intensities reduction were observed for ALA:AuFeNPs bands 1420 and 772 cm^{-1}. These peaks are attributed to the asymmetric and symmetric vibration of the COO– chelating bidentate interaction between ALA and Fe atoms on the surface of the particles.

Figure 4a shows the spherical shape of the ALA:AuNPs by the images of transmission electron microscopy. The spheres present sizes ranging from 15 to 30 nm. Figure 4b shows ALA:AuFeNPs with spheres of around 22 ± 8 nm (AuNPs) surrounded by smaller spheres of around 8 ± 3 nm (FeNPs), in chain-like structure [32].

Table 2 Measured Zeta Potential for ALA:AuNPs and ALA:AuFeNPs nanoparticles

Solutions	Size (nm)	Zeta potential (mV)
ALA:AuNPs pH 7.2	22 ± 8 nm	-23.1 ± 1.0
ALA:AuFeNPs pH 7.3	22 ± 8 nm and 8 ± 3 nm	-29.0 ± 0.8

The stability of ALA:AuNPs and ALA:AuFeNPs was estimated by Zeta Potential measurements (Table 2), and the values were close to − 30 mV, confirming good stability of the nanohybrids.

The cell toxicity of ALA:AuNPs and ALA:AuFeNPs to THP-1 macrophages is shown in Fig. 5a, b respectively. The MTS assay showed that the ALA:AuNPs nanoparticles does not have significant cell toxicity up to 10 µM (Fig. 5a). ALA:AuFeNPs is ~ 7 times more toxic than ALA:AuNPs (Fig. 5b).

M1 macrophages promote formation of complicated and unstable atherosclerotic plaques by maintaining proinflammatory microenvironment. The reduction of macrophages from plaques represents a new strategy for the atherosclerosis treatment [33, 34]. Similarly targeting tumor-associated macrophages (TAMs) is a promising therapeutic strategy for cancer patients [3].

Reports have shown that ALA-conjugated gold allows selective and efficient destruction of cells in the ALA-PDT [35, 36]. To verify if the presence of iron nanoparticles could improve the efficiency of the ALA-mediated PDT, macrophages were incubated with ALA:AuNPs and ALA:AuFeNPs for 24 h and after this time, the macrophages were irradiated with LED at 590 nm by 2 min. The toxicity of cells after PDT treatment was measured using MTS assay and the results are shown in the Fig. 6a, b. Treatment with ALA:AuFeNPs + PDT increased the level of cytotoxicity observed in macrophages in almost 50%, compared with the ALA:AuNPs + PDT treatment group. No cytotoxicity was observed with cells in the presence of PDT and absence of nanoparticles [37].

We believe that the ALA:AuNPs and ALA:AuFeNPs are internalized by the macrophages, and these nanoparticles bypass the natural regulation that heme exerts on ALA synthesis, which leads to increased production of PpIX. We therefore propose that the presence of iron nanoparticles interfere in the selectivity of iron transport across the mitochondrial inner membrane, which culminate in

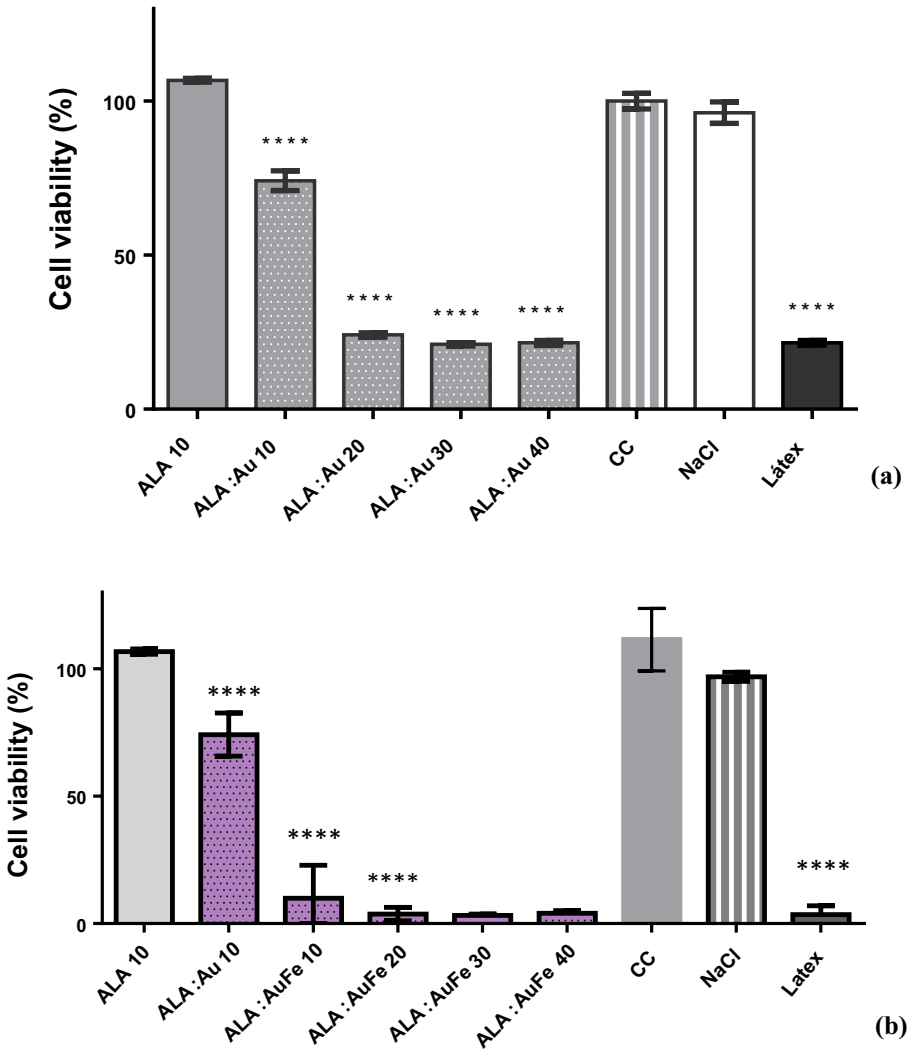

Fig. 5 MTS assay for THP-1 macrophages cells after incubation by 24 h with a) ALA:AuNPs and b) ALA:AuFe. The values of 10 to 40 µL correspond to the volume of NPs added to each well containing cells. The final volume in each well was kept constant adding serum free RPMI-1640. ****P < 0.0001 statistically significant difference from control

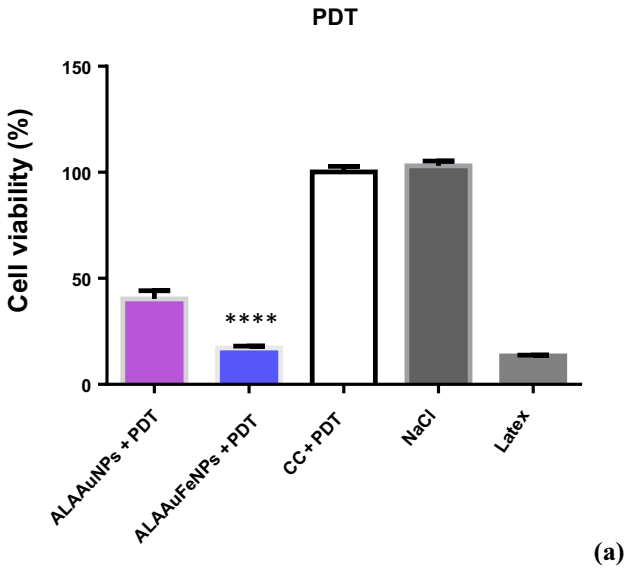

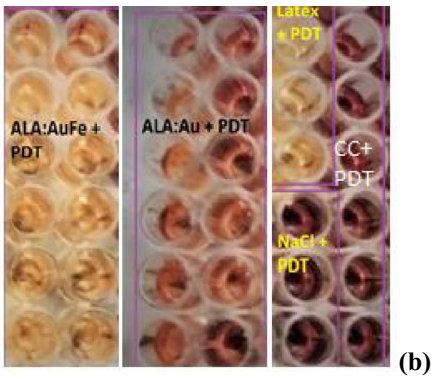

Fig. 6 **a** Viability test after PDT (590 nm, 2 min) of THP-1 macrophages incubated with RPMI-1640 medium (10 µL)—CC + PDT, ALA:AuNPs (10 µL) and ALA:AuFeNPs (10 µL) by 24 h. Negative control (NaCl 0.9%) and positive control (latex). ****$P < 0.0001$ statistically significant difference between ALA:AuNPs and ALA:AuFeNPs. **b** The red wells indicate that the cells did not die. The clearer the tone, the greater the number of dead cells

the decrease of the efficacy of ferrochelatase to convert excessively produced PpIX to heme [38]. So, the accumulation of PpIX increases in the case of ALA:AuFeNPs and improves PDT efficacy.

In this paper it was focused on the strategies for the fabrication of multifunctional nanostructures, combining either the magnetic or the plasmonic properties. Indeed, these nanohybrids can generate heat under an external magnetic field, making them useful for magnetic hyperthermal therapy [5]. Besides, they can be transported close to a specific target for magnetically assisted drug delivery and potentially MRI agent allowing the combination of imaging and therapy in the same nanoparticle.

4 Conclusions

We have synthesized PEGylated ALA:AuFe nanohybrids in aqueous medium by photoreduction method using aminolevulinic acid as reducing, stabilizing and capping agent, rendering the whole procedure cost-effective and environment friendly. With this photoreduction method, the gold-iron nanohybrid is constructed in one-step, in only 5 min. ALA is an endogenous compound and for this reason nontoxic and light irradiation acts as reducing agent. The presence of ALA in the ALA:AuFe nanohybrids composition guaranties delivery to the macrophages. The use of iron powder provides a simple and cost-effective alternative. The stable synthesized nanohybrids have gold particles surrounded by iron nanoparticles in chain-like structure. MTS assay showed that nanohybrids are more toxic than ALA:AuNPs nanoparticles. Treatment with ALA:AuFeNPs + PDT increased the level of cytotoxicity observed in macrophages in almost 50%, compared with the ALA:AuNPs + PDT treatment group. The obtained results indicated that nanohybrids ALA:AuFeNPs offer a new modality for selective and efficient destruction of macrophages and can be a powerful weapon to diagnosis and therapy of non-communicable diseases as cardiovascular diseases and cancer.

Acknowledgements This work was supported by the "Fundação de Amparo a Pesquisa do Estado de São Paulo" (FAPESP), Grant number 2014/06960-9.

Compliance with ethical standards

Conflict of interest The authors declare that they have no conflict of interest.

References

1. G. Sum, T. Hone, R. Atun, C. Millett, M. Suhrcke, A. Mahal, G.C.H. Koh, J.T. Lee, Multimorbidity and out-of-pocket expenditure on medicines: a systematic review. BMJ Glob. Health **3**, e000505 (2018)
2. J.V. Tapia-Vieyra, B. Delgado-Coello, J. Mas-Oliva, Atherosclerosis and cancer; a resemblance with far- reaching implications. Arch. Med. Res. **48**, 12–26 (2017)
3. N. Hayashi, H. Kataoka, S. Yano, M. Tanaka, K. Moriwaki, H. Akashi, S. Suzuki, Y. Mori, E. Kubota, S. Tanida, S. Takahashi, T. Joh, A Novel photodynamic therapy targeting cancer cells and tumor-associated macrophages. Mol. Cancer Ther. **14**, 452–460 (2015)

4. M. Jain, M. Zellweger, A. Frobert, J. Valentin, H. van den Bergh, G. Wagnieres, S. Cook, M.N. Giraud, Intra-arterial drug and light delivery for photodynamic therapy using visudyne (R): implication for atherosclerotic plaque treatment. Front. Physiol. **7**, 400 (2016)
5. Q. Liu, M.R. Hamblin, Macrophage-targeted photodynamic therapy: scavenger receptor expression and activation state. Int. J. Immunopathol. Pharmacol. **18**, 391–402 (2005)
6. B.W. Henderson, T.J. Dougherty, how does photodynamic therapy work. Photochem. Photobiol. **55**, 145–157 (1992)
7. T. Namikawa, T. Yatabe, K. Inoue, T. Shuin, K. Hanazaki, Clinical applications of 5-aminolevulinic acid-mediated fluorescence for gastric cancer. World J. Gastroenterol. **21**, 8769–8775 (2015)
8. F. Tian, J.T. Yao, M. Yan, X. Sun, W. Wang, W.W. Gao, Z. Tian, S.Y. Guo, Z.X. Dong, B.C. Li, T.L. Gao, P. Shan, B. Liu, H.Y. Wang, J.L. Cheng, Q.P. Gao, Z.G. Zhang, W.W. Cao, Y. Tian, 5-aminolevulinic acid-mediated sonodynamic therapy inhibits RIPK1/RIPK3-dependent necroptosis in THP-1-derived foam cells. Sci. Rep. **6**, 21992 (2016)
9. S.Y. Guo, X. Sun, J.L. Cheng, H.B. Xu, J.H. Dan, J. Shen, Q. Zhou, Y. Zhang, L.L. Meng, W.W. Cao, Y. Tian, Apoptosis of THP-1 macrophages induced by protoporphyrin IX-mediated sonodynamic therapy. Int. J. Nanomed. **8**, 2239–2246 (2013)
10. L.B. Zheng, X.Y. Sun, X. Zhu, F.X. Lv, Z.Y. Zhong, F. Zhang, W.H. Guo, W.W. Cao, L.M. Yang, Y. Tian, Apoptosis of THP-1 derived macrophages induced by sonodynamic therapy using a new sonosensitizer hydroxyl acetylated curcumin. PLoS ONE **9**, e93133 (2014)
11. L.B. Sicchieri, M.N. Da Silva, R.E. Samad, L.C. Courrol, Can measurement of the fluorescence lifetime of extracted blood PPIX predict atherosclerosis? J. Lumin. **195**, 176–180 (2018)
12. K.C. Blanco, L.T. Moriyama, N.M. Inada, A.G. Salvio, P.F.C. Menezes, E.J.S. Leite, C. Kurachi, V.S. Bagnato, Fluorescence guided PDT for optimization of the outcome of skin cancer treatment. Front. Phys. **3**, 30 (2015)
13. T. Feuerstein, G. Berkovitch-Luria, A. Nudelman, A. Rephaeli, Z. Malik, Modulating ALA-PDT efficacy of mutlidrug resistant MCF-7 breast cancer cells using ALA prodrug. Photochem. Photobiol. Sci. **10**, 1926–1933 (2011)
14. Y. Tian, C. Peng, X. Sun, J. Cheng, L. Yang, J. Wu, Z. Zhang, W. Cao, 5-aminolevulinic acid-derived protoporphyrin ix mediated fluorescence diagnosis and photodynamic therapy of macrophages within the atherosclerotic plaque. Atheroscler. Suppl. **12**, 160 (2011)
15. M.K.K. Oo, X. Yang, H. Du, H. Wang, 5-aminolevulinic acid-conjugated gold nanoparticles for photodynamic therapy of cancer. Nanomedicine **3**, 777–786 (2008). https://doi.org/10.2217/17435889.3.6.777
16. K.D. Goncalves, D.P. Vieira, L.C. Courrol, Synthesis and characterization of aminolevulinic acid gold nanoparticles: photo and sonosensitizer agent for atherosclerosis. J. Lumin. **197**, 317–323 (2018)
17. P. E. Chow, in *Gold nanoparticles properties, characterization and fabrication*. Nanotechnology science and technology series (Nova Science Publishers, 2010), pp. 1 online resource (xvi, p. 343)
18. P.K. Jain, X. Huang, I.H. El-Sayed, M.A. El-Sayad, Review of some interesting surface plasmon resonance-enhanced properties of noble metal nanoparticles and their applications to biosystems. Plasmonics **2**, 107–118 (2007)
19. C. Yao, L. Zhang, J. Wang, Y. He, J. Xin, S. Wang, H. Xu, Z. Zhang, Gold nanoparticle mediated phototherapy for cancer. J. Nanomater. **2016**, 5497136 (2016). https://doi.org/10.1155/2016/5497136
20. C. Louis, EBSCO Publishing (Firm), and O. Pluchery, "*Gold nanoparticles for physics, chemistry and biology*," p. 1 online resource (406 pages)
21. N. Aich, J. Plazas-Tuttle, J.R. Lead, N.B. Saleh, A critical review of nanohybrids: synthesis, applications and environmental implications. Environ. Chem. **11**, 609–623 (2014)
22. H. Zhou, F. Zou, K. Koh, J. Lee, Multifunctional magnetoplasmonic nanomaterials and their biomedical applications. J. Biomed. Nanotechnol. **10**, 2921–2949 (2014)
23. A.O. Baskakov, A.Y. Solov'eva, Y.V. Ioni, S.S. Starchikov, I.S. Lyubutin, I.I. Khodos, A.S. Avilov, S.P. Gubin, Magnetic and interface properties of the core-shell Fe3O4/Au nanocomposites. Appl. Surf. Sci. **422**, 638–644 (2017)
24. T.T. Nguyen, F. Mammeri, S. Ammar, Iron oxide and gold based magneto-plasmonic nanostructures for medical applications: a review. Nanomaterials **8**, 149 (2018)
25. J. Gautier, E. Allard-Vannier, E. Munnier, M. Souce, I. Chourpa, Recent advances in theranostic nanocarriers of doxorubicin based on iron oxide and gold nanoparticles. J. Control. Release **169**, 48–61 (2013)
26. P. Wagener, J. Jakobi, C. Rehbock, V.S.K. Chakravadhanula, C. Thede, U. Wiedwald, M. Bartsch, L. Kienle, S. Barcikowski, Solvent-surface interactions control the phase structure in laser-generated iron-gold core-shell nanoparticles. Sci. Rep. **6**, 23352 (2016)
27. R.A. de Matos, L.C. Courrol, Biocompatible silver nanoparticles prepared with amino acids and a green method. Amino Acids **49**, 379–388 (2017)
28. C.R.B. Lopes, L.C. Courrol, Green synthesis of silver nanoparticles with extract of Mimusops coriacea and light. J. Lumin. **199**, 183–187 (2018)
29. P. Kshirsagar, S.S. Sangaru, M.A. Malvindi, L. Martiradonna, R. Cingolani, P.P. Pompa, Synthesis of highly stable silver nanoparticles by photoreduction and their size fractionation by phase transfer method. Colloids Surf a-Physicochem Eng Aspects **392**, 264–270 (2011)
30. Z.Y. Qin, The use of THP-1 cells as a model for mimicking the function and regulation of monocytes and macrophages in the vasculature. Atherosclerosis **221**, 2–11 (2012)
31. Khairuddin, E. Pramono, S. B. Utomo, V. Wulandari, A. Zahrotul, and F. Clegg, FTIR studies on the effect of concentration of polyethylene glycol on polimerization of Shellac. in *8th International conference of physics and its applications (ICOPIA)*(Denpasar, INDONESIA, 2016)
32. D.F. Zhang, Q. Zhang, L.Y. Niu, L. Jiang, P.G. Yin, L. Guo, Self-assembly of gold nanoparticles into chain-like structures and their optical properties. J. Nanoparticle Res. **13**, 3923–3928 (2011)
33. F.P. Wang, Q.P. Gao, S.Y. Guo, J.L. Cheng, X. Sun, Q.N. Li, T.Y. Wang, Z.G. Zhang, W.W. Cao, Y. Tian, The sonodynamic effect of curcumin on THP-1 cell-derived macrophages. Biomed Res. Int. (2013). https://doi.org/10.1155/2013/737264
34. X. Zhu, H. Wang, L.B. Zheng, Z.Y. Zhong, X.S. Li, J. Zhao, J.Y. Kou, Y.Q. Jiang, X.F. Zheng, Z.N. Liu, H.X. Li, W.W. Cao, Y. Tian, Y. Wang, L.M. Yang, Upconversion nanoparticle-mediated photodynamic therapy induces THP-I macrophage apoptosis via ROS bursts and activation of the mitochondrial caspase pathway. Int. J. Nanomed. **10**, 3719–3736 (2015)
35. Z. Zhang, Y.S. Chen, J.Y. Ding, C.L. Zhang, A. Zhang, D.N. He, Y.X. Zhang, Biocompatible 5-aminolevulinic Acid/Au nanoparticle-loaded ethosomal vesicles for in vitro transdermal synergistic photodynamic/photothermal therapy of hypertrophic scars. Nanoscale Res. Lett. **12**, 622 (2017)

36. K.D. Goncalves, M.N. da Silva, L.B. Sicchieri, F.R.D. Silva, R.A. de Matos, L.C. Courrol, Aminolevulinic acid with gold nanoparticles: a novel theranostic agent for atherosclerosis. Analyst **140**, 1974–1980 (2015)
37. L.L. Xin, J.S. Wang, G.Q. Fan, B.Z. Che, Y.H. Wu, S.F. Guo, J. Tong, Oxidative stress and mitochondrial injury-mediated cytotoxicity induced by silver nanoparticles in human A549 and HepG2 Cells. Environ. Toxicol. **31**, 1691–1699 (2016)
38. H. Lange, G. Kispal, R. Lill, Mechanism of iron transport to the site of heme synthesis inside yeast mitochondria. J. Biol. Chem. **274**, 18989 (1999)